frontiers in Marine Science

ORIGINAL RESEARCH
published: 07 February 2022
doi: 10.3389/fmars.2022.819340

Sediment Resuspension as a Major Contributor to Sinking Particles in the Northwestern South China Sea: Evidence From Observations and Modeling

Lihua Ran[1,2,3], Wentao Ma[2,3], Martin G. Wiesner[2], Yuntao Wang[2], Jianfang Chen[1,2]*, Lanlan Zhang[4], Zhi Yang[1], Jingjing Zhang[1], Hongliang Li[1], Jian Ren[1], Rong Xiang[4] and Erick Fredj[5]*

[1] Key Laboratory of Marine Ecosystem Dynamics, Ministry of Natural Resources, Hangzhou, China, [2] State Key Laboratory of Satellite Ocean Environment Dynamics, Second Institute of Oceanography, Ministry of Natural Resources, Hangzhou, China, [3] Southern Marine Science and Engineering Guangdong Laboratory (Zhuhai), Zhuhai, China, [4] Key Laboratory of Ocean and Marginal Sea Geology, Chinese Academy of Sciences, Guangzhou, China, [5] Department of Computer Science, Jerusalem College of Technology, Jerusalem, Israel

The lateral advection of sinking particles is a well-known phenomenon in the South China Sea (SCS) and has a significant impact on the estimation of the efficiency of the biological carbon pump. However, little is known about the sources and pathways of sinking particles. Here, we present benthic and freshwater diatom fluxes and relative abundances collected by a sediment trap deployed at a water depth of 1,000 m and more than 500 m above the seafloor in the northwestern SCS, indicating that laterally transported resuspended sediment accounts for a significant part of the particle flux to the deep sea. A Lagrangian particle tracking model (LPTM) revealed that the resuspended particles likely originated from the neighboring continental slope, approximately 12–145 km to the west of the study site. Sediment trap observations and the LPTM together indicated that the impact of resuspended sediment occurred mainly in the deep water, and especially strong sediment resuspension was related to summer monsoon-induced coastal upwelling. The results suggest that particle resuspension has an important impact on the biological pump as well as on paleoenvironmental reconstructions of the SCS.

Keywords: sediment trap, diatom, Lagrangian particle tracking model, sediment resuspension, South China Sea

OPEN ACCESS

Edited by:
Laurent Coppola, UMR 7093 Laboratoire d'Océanographie de Villefranche (LOV), France

Reviewed by:
Yuan-Pin Chang, National Sun Yat-sen University, Taiwan
Frédéric André Corentin Le Moigne, UMR 6539 Laboratoire des Sciences de l'Environnement Marin (LEMAR), France

****Correspondence:***
Lihua Ran
lihuaran@sio.org.cn
Jianfang Chen
jfchen@sio.org.cn

Specialty section:
This article was submitted to Ocean Observation, a section of the journal Frontiers in Marine Science

Received: *21 November 2021*
Accepted: *17 January 2022*
Published: *07 February 2022*

Citation:
Ran L, Ma W, Wiesner MG, Wang Y, Chen J, Zhang L, Yang Z, Zhang J, Li H, Ren J, Xiang R and Fredj E (2022) Sediment Resuspension as a Major Contributor to Sinking Particles in the Northwestern South China Sea: Evidence From Observations and Modeling. Front. Mar. Sci. 9:819340. doi: 10.3389/fmars.2022.819340

INTRODUCTION

Sediment traps are used as an effective tool for monitoring marine organic carbon export, i.e., the biological carbon pump, by collecting time-series sinking particles in the deep ocean, which are the major carrier of organic carbon from the surface ocean to the deep sea. Earlier studies have assumed one-dimensional particle settling to link surface ocean properties, e.g., primary productivity, with

the deep water fluxes of particulate matter (Honjo et al., 2008). However, as particles sink to the deep ocean, horizontal advection of water may significantly displace particles from their original location (Siegel and Deuser, 1997; Waniek et al., 2000, 2005; Wekerle et al., 2018) and lead to bias in evaluations of the biological carbon pump (Deuser et al., 1990). The trajectories of particle transport between the location of a sediment trap and the region of particle sources largely depend on the horizontal velocity field, the particle sinking velocity, and the depth of the trap (Siegel and Deuser, 1997; Waniek et al., 2000, 2005; Siegel et al., 2008; Wekerle et al., 2018). Therefore, traps moored at a given site but different depths can collect particles originating from different sources, which in turn may vary both by season and by year.

The South China Sea (SCS), as the largest marginal sea of the western Pacific, has attracted widespread attention in ocean research (Wang P. et al., 2015). Due to the strong influence of the East Asian monsoon, the surface circulation exhibits clear seasonality, especially in the northern SCS (e.g., Wyrtiki, 1961; Hu et al., 2000). In general, basin-wide cyclonic circulation occurs in response to the northeast monsoon in the winter, while anticyclonic circulation occurs mainly in the southern SCS in response to the southwest monsoon in the summer (Hu et al., 2000). This significant seasonal environmental variation results in seasonal changes in the upper ocean nutrient content, primary productivity, and organic carbon export (Liu et al., 2002, 2013; Ran et al., 2015a,b; Li et al., 2017). Moreover, monsoon-induced upwelling, mesoscale eddies, internal solitary waves (ISWs), typhoons, and atmospheric dust deposition frequently influence the SCS, resulting in highly complicated and variable marine environments and biogeochemical processes in the SCS (e.g., Wang et al., 2012, 2016, 2018; Zhou et al., 2013; Li et al., 2017; Yu et al., 2019, 2020; Zhang et al., 2019). To understand the complex biogeochemical processes and biological carbon pump in the SCS, bottom-tethered sediment traps have been widely used since the 1980s, particularly in the northern and central parts of the basin (Wiesner et al., 1996; Lahajnar et al., 2007; Gaye et al., 2009; Ran et al., 2015a,b; Li et al., 2017; Zhang et al., 2019; Tan et al., 2020).

The clear impact of lateral particle transport on sinking particle fluxes in the deep SCS has been investigated using sediment trap observations (Chen, 2005; Liu et al., 2014; Ran et al., 2015a,b; Dong et al., 2016; Priyadarshani et al., 2019). In addition, lateral advection can not only significantly displace particles from their original location during sinking but also transport resuspended sediment from continental margins into the deep ocean (e.g., Priyadarshani et al., 2019; Ma et al., 2021), which increases the complexity of particle composition. Shen et al. (2020) showed that laterally transported particles from continental margins serve as major sources of carbon (60 ± 11% below 100 m and 85 ± 14% below 374 m in the northern SCS) and energy for the deep ocean ecosystems in the SCS. Nevertheless, little is known about the specific sources and transport pathways of the laterally transported particles entering the deep SCS.

In recent years, a Lagrangian particle tracking algorithm with a high-resolution velocity field was applied to determine the catchment area of a bottom-tethered time-series sediment trap (e.g., Wekerle et al., 2018). Particles were treated as if they rose from the mooring location to the surface with a negative settling velocity and were horizontally displaced with the reversed horizontal velocity. In the northern SCS, Ma et al. (2021) employed a Lagrangian particle tracking model (LPTM) forced by the three-dimensional currents of eddy composites derived from the Global Hybrid Coordinate Ocean Model (HYCOM) to study the role of eddies in the lateral transport of sinking particles. According to their findings, the trap-collected slow-sinking particles (sinking velocity = 5 $m \cdot day^{-1}$) may have originated from the subsurface tens to hundreds of kilometers from the trap location.

In an earlier study, extremely high contents of lithogenic matter in the sinking particles were observed by sediment traps in the northwestern SCS subbasin (Zhang et al., 2019), which suggested that resuspended sediment was a possible source of settling particles. However, little is known about the source and trajectories of these resuspended sediments as well as the importance of resuspended sediment contributing to the sinking particles in the SCS. In this paper, (1) diatoms in the sinking particles collected by sediment traps in the northwestern SCS were analyzed to better understand the potential source of sinking particles, and (2) the LPTM was utilized to trace the sources and identify the transport pathways of the sinking particles, especially the resuspended sediment in the sinking particles, in the northwestern SCS subbasin.

MATERIALS AND METHODS

Sampling of Sinking Particles

The sediment trap (Mark78H-21, McLane) was deployed at station SCS-NW in the northwestern SCS subbasin (**Figure 1**, with one trap mounted at a depth of 1,000 m at 17°25.8′N, 110°40.2′E; total water depth was 1,548 m) from July 2012 to April 2013. In total, 16 sinking particle samples were collected by the sediment trap. The variations in the total particle fluxes (TPFs, $mg \cdot m^{-2} \cdot day^{-1}$) of the sinking particles collected by the sediment trap and fluxes of the main chemical components, i.e., biogenic opal, calcium carbonate ($CaCO_3$), organic matter and lithogenic matter, in the sinking particles were described in Zhang et al. (2019).

Diatom Analysis

For each sample, approximately 5–6 mg of well-mixed and freeze-dried particles was used for diatom analysis. The samples were precisely weighed with a precision of 0.1 mg. The chemical treatment was applied and permanent slides were prepared for microscopic observations according to Ran et al. (2015a). Hydrochloric acid (HCl) (10%) and hydrogen peroxide (H_2O_2) (30%) were added to the sample and heated to remove calcareous and organic matter. After complete digestion, the mixture was carefully stirred with distilled water and kept for 24 h to settle the particles. Subsequently, the supernatant was removed by a cycle of syphoning and washing four times to remove redundant HCl and H_2O_2 and the reaction solution. The remaining sample was diluted to 20 ml, and then 2 ml of gelatin solution was added

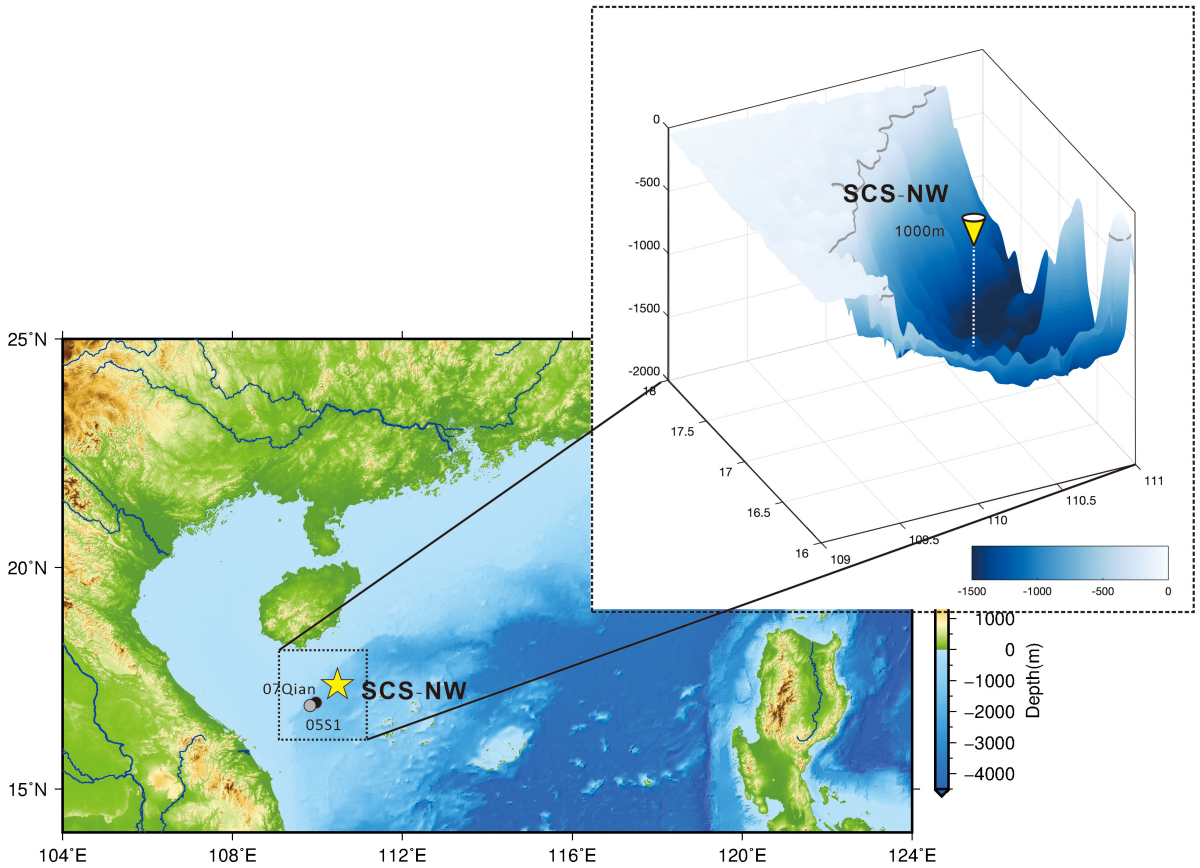

FIGURE 1 | Site location of the sediment trap station and the sketch diagram of the sediment trap mooring in the northwestern SCS.

to accelerate the following settlement process. The well-mixed sample solution was gently decanted into a petri dish, in which two 24 mm × 24 mm cover slips were fixed beforehand. After 24 h of settling, the supernatant in the dish was removed by a strip of absorptive paper. When the material was completely dried, the cover slips were transferred onto a labeled slide and mounted with Naphrax (dn = 1.72). A phase-contrast microscope (Motic BA410) was used to count and identify diatoms at 1,000 × magnification. The sinking fluxes of diatoms (valves·m^{-2}·day^{-1}) and relative abundances of diatom species and groups were calculated.

$$f = \frac{N \times A \times F}{n \times a \times m}$$

where f is the diatom flux (valves·m^{-2}·day^{-1}), N is the number of diatoms counted under a microscope, A is the area of the petri dish, F is the TPF (mg·m^{-2}·day^{-1}), n is the number of fields of vision counted for diatoms under the microscope, a is the area of one field of vision, and m is the weight of the sample (mg) used for diatom analysis.

Lagrangian Particle Tracking Model

The LPTM was used to calculate the sources and trajectories of the sinking particles collected by the sediment trap at a water depth of 1,000 m during five selected periods, i.e., August 6 to 21, September 5 to 20, October 5 to 20, and November 19 to December 14 in 2012 and February 2 to March 4 in 2013, which were chosen because of the TPF maxima and minima (Zhang et al., 2019). The movement of particles was tracked using the HYCOM reanalysis product of expt_53.X[1], which has a horizontal resolution of ∼0.08° and 41 vertical layers. The HYCOM model uses the Navy Coupled Ocean Data Assimilation (NCODA) system for data assimilation (Cummings and Smedstad, 2013). The validation of HYCOM outputs against remote sensing data, Argo profiles, and drifter observations for the SCS was reported in Yan et al. (2019). Overall, the modeled temperature, salinity and current agree with the observations very well in all seasons (see Figures A1–A4 in Yan et al., 2019). The application of HYCOM outputs for the analysis of ocean circulation was performed in the northeastern and western SCS (Zhang et al., 2010; Wang A. et al., 2015; Yan et al., 2019).

The LPTM toolbox PATATO was used to perform backward tracking (Fredj et al., 2016). On each day, 1,000 particles were released from 1,000 m with sinking velocities of 50, 100, and 200 m·day^{-1}, which were adopted from the literature and considered to be realistic for the bulk material collected by

[1]https://www.hycom.org/data/glbv0pt08/expt-53ptx

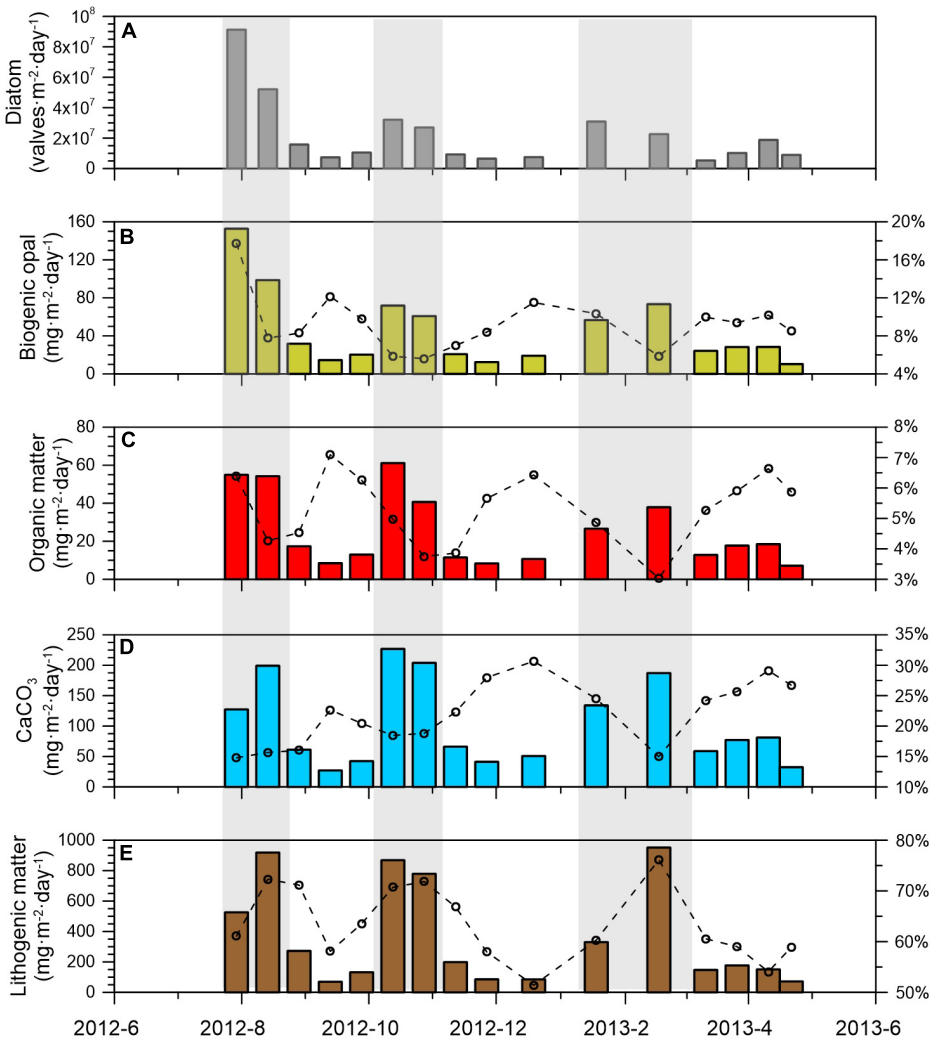

FIGURE 2 | Time-series variations of **(A)** the fluxes of diatoms, fluxes (bars) and proportions (dashed lines) of **(B)** biogenic opal, **(C)** organic matter, **(D)** $CaCO_3$, and **(E)** lithogenic matter (gray bars indicate the three TPF peaks).

sediment traps (Waniek et al., 2000). Particles were tracked backward until they reached the sea surface or impinged on the seafloor because bathymetry was considered in the model. The detailed backtracking algorithm is described in Fredj et al. (2016) and Ma et al. (2021).

Auxiliary Data

Additional datasets were used to help interpret the data collected in this study. Two surface sediment samples near station SCS-NW (**Figure 1**; 07Qian, 17.2°N, 110.34°E, 1,366 m; 05S1, 17.16°N, 110.27°E, 1,330 m) collected by a box corer were provided by the Key Laboratory of Ocean and Marginal Sea Geology, Chinese Academy of Sciences. The main chemical components and diatom assemblages in the surface sediment were analyzed as a reference for the resuspended sediment from the neighboring seafloor. The analysis of the main chemical components of the surface sediment followed the method described in see section "Diatom Analysis" in Zhang et al. (2019). Data on dust deposition within a 2 × 2° area (16.5°–18.5° N, 109.5°–111.5° E) around station SCS were downloaded from Giovanni, which is managed by the Goddard Earth Sciences Data and Information Services Center (GES DISC). These data were used to estimate the contribution of dust deposition to the lithogenic matter collected in the sediment trap.

RESULTS

Diatoms in the Sinking Particles

The diatom fluxes varied from 0.5 to 9.1 × 10^7 valves·m^{-2}·day^{-1}, generally following the variations in the TPFs and fluxes of the primary components (biogenic opal, organic matter, $CaCO_3$, and lithogenic matter, Zhang et al., 2019), with

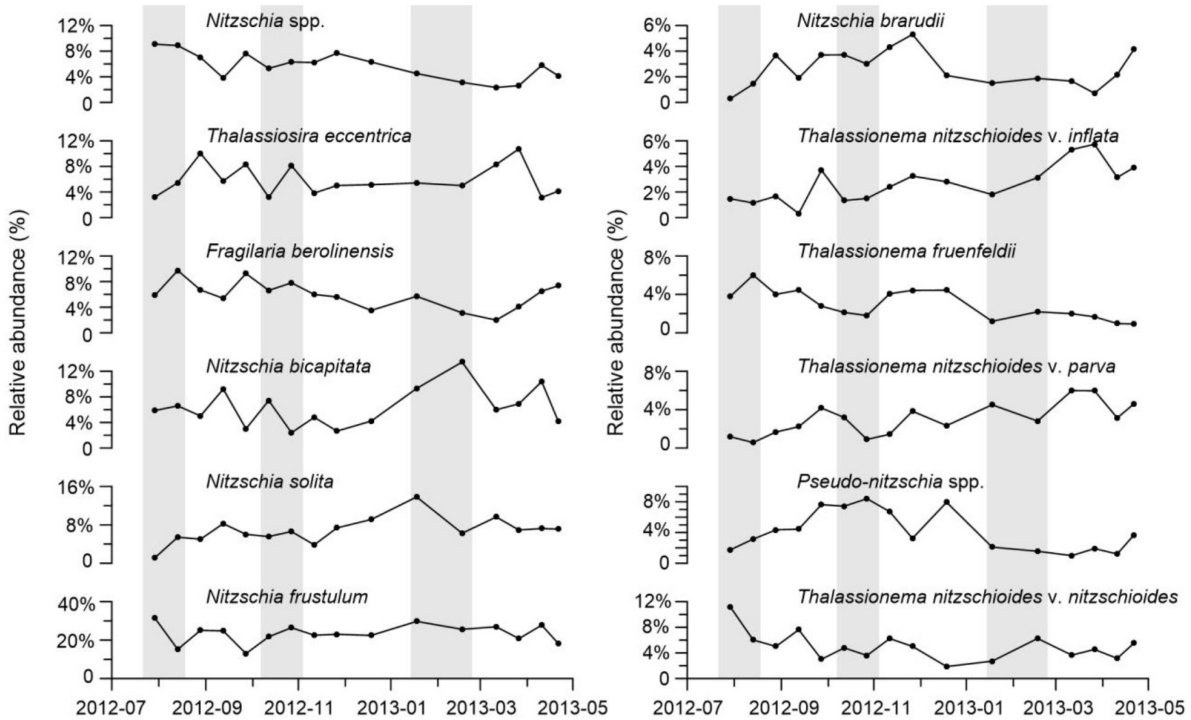

FIGURE 3 | Time-series variation in the relative abundances of the main diatom species (gray bars indicate the three TPF peaks).

three flux peaks identified in the summer, autumn, and winter (**Figure 2** and **Supplementary Dataset 1**). Among the three flux peaks, the first peak in the summer of 2012 was especially outstanding, and the diatom flux in this period was approximately twice as high as the other two flux peaks. This especially high flux of diatoms corresponded to an especially high flux of biogenic opal (**Figure 2B**); however, variations in organic matter, $CaCO_3$, and lithogenic matter fluxes were not observed. Lithogenic matter was the dominant component of sinking particles at 1,000 m, contributing 63.4 ± 7.3% to the total particle flux. The proportion of lithogenic matter was generally high during the high flux periods, and the other chemical components were diluted by lithogenic matter.

The variations in diatom species with a relative abundance >2% are plotted in **Figure 3** (see details in **Supplementary Dataset 2**). *Nitzschia*, including *N. frustulum*, *N. bicapitata*, *N. solita*, *N. brarudii*, etc., was the most common diatom species in the sinking particles, contributing 42.4–65.5% of the diatom flora in the northwestern SCS. *N. frustulum* was the dominant diatom species. *Thalassionema nitzschioides*, including its varieties, i.e., var. *parva* and var. *inflata*, *Thalassiosira eccentrica*, *Fragilaria berolinensis*, and *Pseudo-nitzschia* spp. were also common. The temporal variations in the relative abundances of different diatom species are shown in **Figure 3**; however, there was no obvious seasonal variation pattern for specific diatom species. Additionally, no apparent correlation between the variation in diatom species relative abundance and the variation in diatom fluxes was distinguished.

A group of benthic diatoms, such as *Diploneis* spp., *Pleurosigma* spp., *Paralia sulcata*, and *Triceratium cinnamomeum*, and freshwater diatoms, such as *Fragilaria* spp. and *Achnanthes* spp., were frequently found in the SCS-NW trap, although in relatively low abundances (total of 1.5–6.9%). Interestingly, the variations in the fluxes and relative abundance of the benthic and freshwater diatoms generally followed the variation in the total diatom fluxes (**Figure 4**). In particular, the highest fluxes and relative abundance of benthic and freshwater diatoms were found in August 2012 (6.9%), when the fluxes of diatoms and biogenic opal were especially high.

Backtracking of Sinking Particles

The local source regions of the sinking particles in three periods of diatom flux maxima (August 6 to 21 and October 5 to 20 in 2012 and February 2 to March 4 in 2013) and two periods of flux minima (September 5 to 20 and November 19 to December 14 in 2012) were determined by the LPTM (see details in **Supplementary Dataset 3**). The positions where the particles reached the sea surface or impinged on the seafloor are shown in **Figure 5**.

Clear seasonality was observed in the sinking particle source regions, which generally followed the seasonal change in the sea surface current field (**Figure 6**). During the southwest monsoon period in August 2012, most of the particles originated from the southwest and west of the station as the sea surface current was generally from southwest to the northeast. During the monsoon transition period (September 5 to 20) when the surface current velocity decreased significantly, particles came from southwest

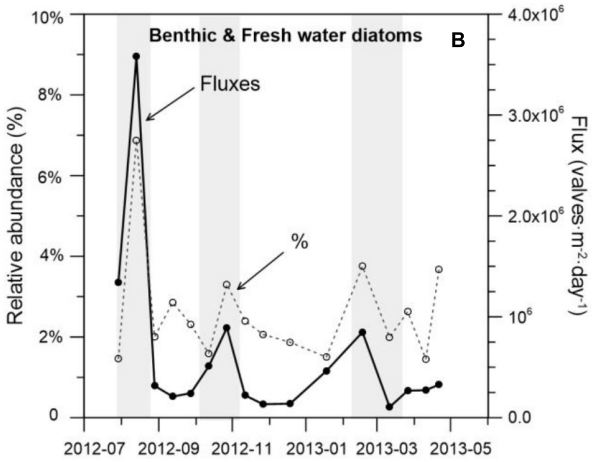

FIGURE 4 | Time-series variation in the fluxes and relative abundances of benthic and freshwater diatoms (gray bars indicate the three TPF peaks).

and south of the trap. In October 2012 (at the onset of the northeast monsoon), particles originated from a large area along the continental shelf break to the northeast and southwest of the trap location, corresponding to the strong sea surface current from the northeast to the southwest in the coastal area off Hainan. From November to December 2012, when the monsoon attains its maximum strength and the sea surface currents flowed from east and northeast to west, particles were generally from the east of the trap location. From February to March 2013, when the sea surface wind started to switch from northeasterly to southwesterly directions and the sea surface current velocity became much weaker, most of the particles originated from the south of the trap (as in September 2012).

In addition, apparent differences in the sinking particle source regions were indicated in the LPTM results with different sinking velocities. In general, the catchment area of sinking particles gradually decreased with increasing particle sinking velocity (from the upper panel to the lower panel in **Figure 5**). In particular, the LPTM result obtained with a sinking velocity of 50 m·day^{-1} showed that some particles released from 1,000 m did not arrive at the sea surface but impinged on the continental slope to the west at depths of 300–900 m (**Figure 7**). However, all the particles released with sinking velocities of 100 and 200 m·day^{-1} reached the sea surface. The probability of particles released at 1,000 m with sv = 50 m·day^{-1} reaching the continental slope varied in the range of 4.5–11.7%, with the highest probability in August (**Figure 7A**).

DISCUSSION

Resuspended Sediment From the Continental Slope as a Source of Sinking Particles

As shown in **Figure 4**, benthic and freshwater diatoms were frequently found in the sinking particles. Benthic diatoms are

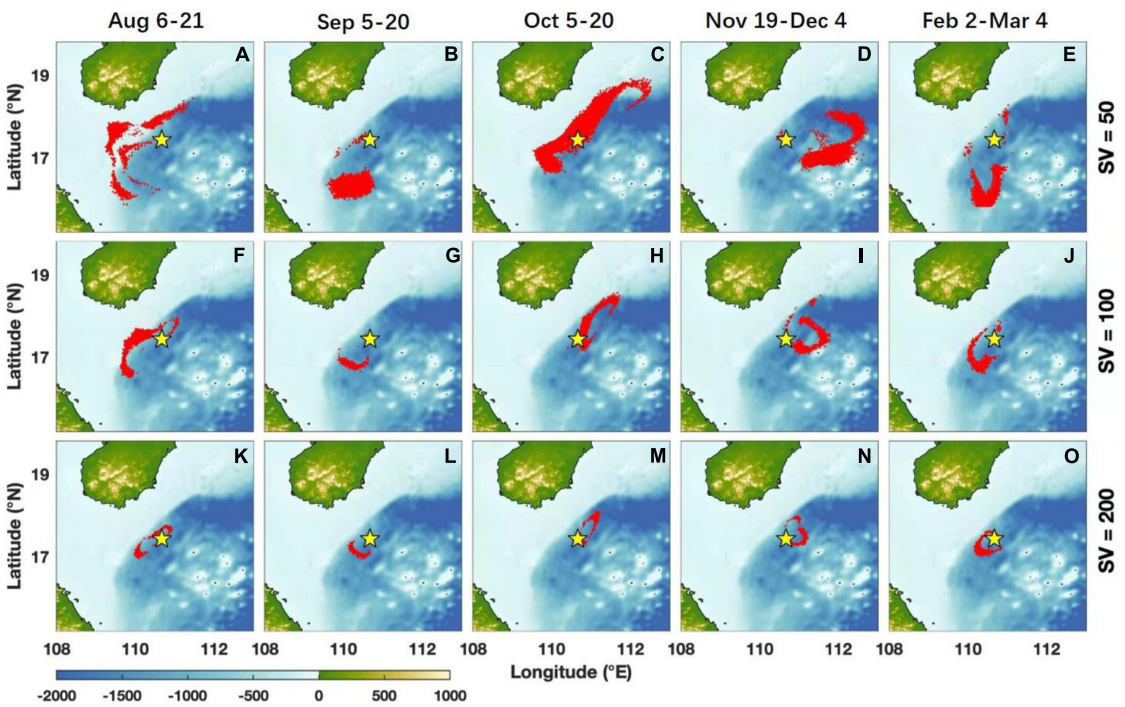

FIGURE 5 | Source regions calculated by LPTM backtracking for sinking particles released at a water depth of 1,000 m with different sinking velocities (sv) (upper panel **A–E**: sv = 50 m·day^{-1}; middle panel **F–J**: sv = 100 m·day^{-1}; and lower panel **K–O**: sv = 200 m·day^{-1}).

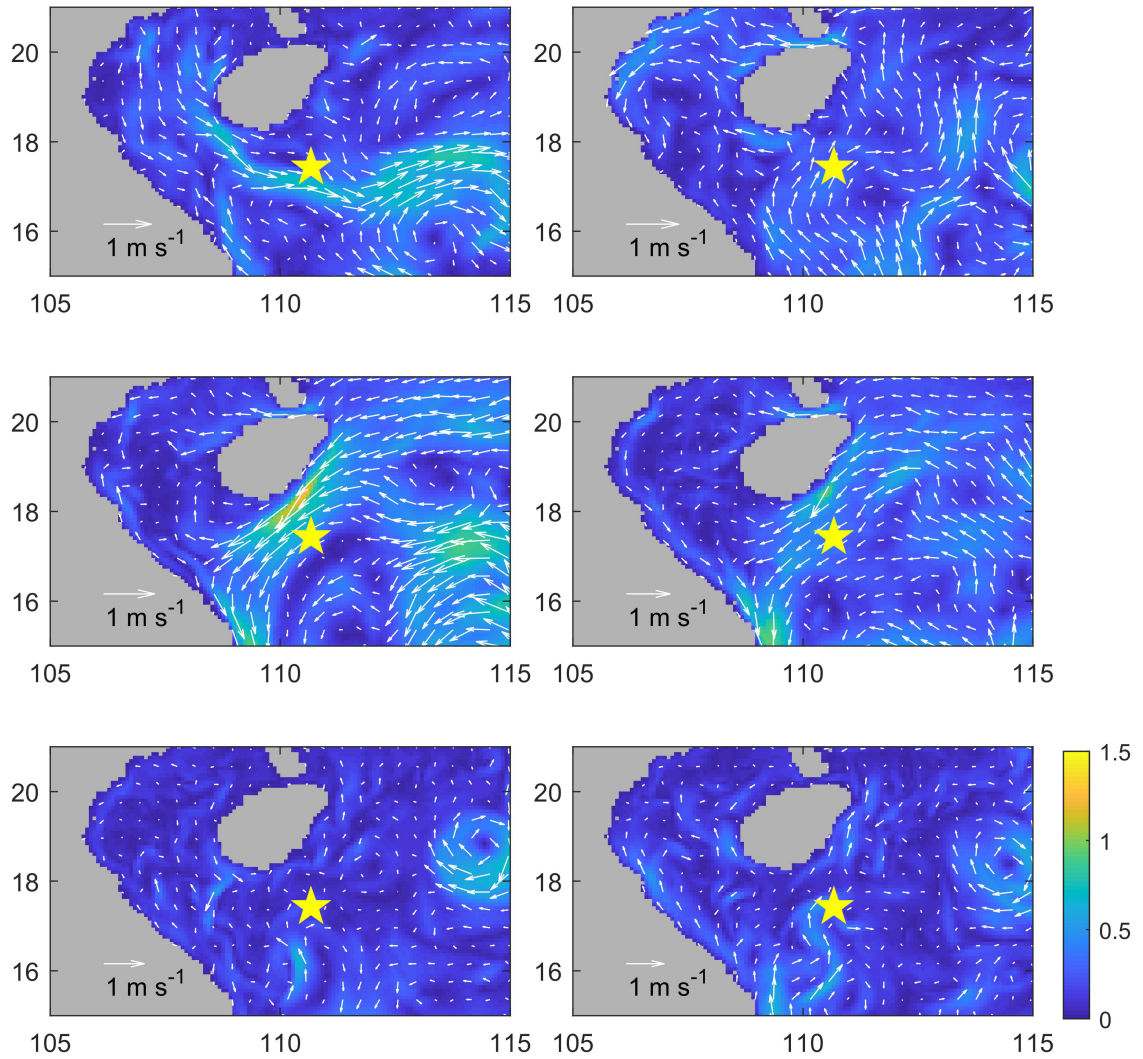

FIGURE 6 | Sea surface current field (data from the HYCOM reanalysis product) in the study area on **(A)** August 6, 2012, **(B)** September 5, 2012, **(C)** October 5, 2012, **(D)** November 19, 2012, **(E)** February 2, 2013, and **(F)** February 17, 2013.

the main primary producers in shallow water and coastal environments and normally live on the seafloor or are attached to benthic plants or animals, and freshwater diatoms are primary producers in fresh waters, such as rivers and lakes. The frequent appearance of benthic diatoms indicated that some particles originated from the seafloor of coastal areas and the shallow continental shelf, and the frequent appearance of freshwater diatoms indicated that some sinking particles originated from the nearshore estuarine area. There are several small rivers draining Hainan Island that may serve as potential sources of freshwater diatoms collected in the sediment trap. The Wanquan River flows eastward into the northwestern SCS. However, a very small daily discharge of ∼100 $m^3 \cdot s^{-1}$ (Wu et al., 2013) and the generally high salinity of the water along the east coast of Hainan (Herbeck et al., 2013; Chen et al., 2020) suggest a very limited impact of Wanquan River runoff in the Hainan coastal area and the northwestern SCS. In addition, the LPTM results indicate that the source region of the sinking particles was generally far from the coast of Hainan Island in the whole sampling year (**Figure 5**). Therefore, freshwater and benthic diatoms may not be directly transported from estuarine and coastal waters. On the other hand, the frequent appearance of freshwater and benthic diatoms in the surface sediment (∼7.8%, **Figure 1** and **Supplementary Dataset 4**) near station SCS-NW suggest that the resuspended sediment near the trap location was another potential source of the freshwater and benthic diatoms collected in the sediment traps.

As shown in **Figure 2E**, lithogenic matter was the dominant component of sinking particles at 1,000 m, contributing 63.4 ± 7.3% to the total particle flux. Fluvial sediment, dust deposition and sediment resuspension were the main potential contributors of the sinking lithogenic particles in the study area. As discussed before, the nearest river runoff from Hainan Island was very limited, and dust deposition (dry + wet) in the study area (16.5°–18.5° N, 109.5°–111.5° E) was 1.7 ± 0.7 $mg \cdot m^{-2} \cdot d^{-1}$,

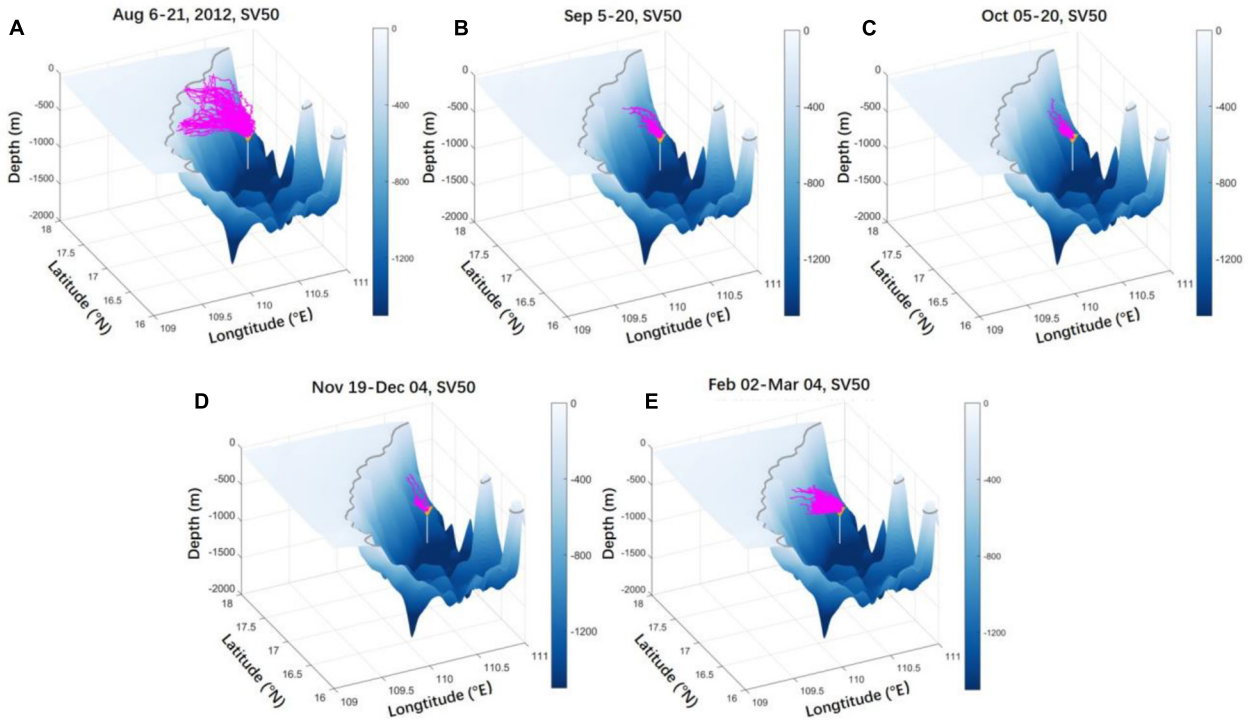

FIGURE 7 | Backtracking of particles released at a water depth of 1,000 m with sv = 50 m·day^{-1} and reaching the continental slope **(A)** from August 6 to 21, **(B)** from September 5 to 20, **(C)** from October 5 to 20, and **(D)** from November 19 to December 4 of 2012, and **(E)** from February 2 to March 4 of 2013.

which contributed only ∼0.45% of the lithogenic matter collected in the sediment trap (360.2 ± 331.8 mg·m^{-2}·d^{-1}). On the other hand, the content of lithogenic matter in sinking particles in the northwestern SCS traps was much higher than that in the northern SCS basin (22.7 ± 10.3% at ∼1,000 m, Ran et al., 2015a; Tan et al., 2020) and the central SCS basin (26.5 ± 9.2% at ∼1,000 m, Li et al., 2017) but closer to the lithogenic matter content in the surface sediment near the SCS-NW trap location in the northwestern SCS (75.2 and 79.2%, data in **Supplementary Dataset 4**). Therefore, the resuspended surface sediment near the trap location was likely one of the most important sources of the sinking particles collected in the sediment trap.

The LPTM results showed that some particles with a relatively low sinking velocity (sv = 50 m·day^{-1}) originated from the continental slope at depths of ∼300–900 m, ∼12–145 km to the west of the SCS-NW station (**Figure 7**). The continental slope to the west of the SCS-NW station was the source region of the resuspended particles collected in the sediment trap. In contrast to the apparent seasonal variation in particle sources at the sea surface in response to monsoon-driven changes in sea surface wind and current directions (**Figures 5**, **6**), the resuspended particles originated from a relatively restricted area on the continental slope. In addition, no significant difference in the probability of particles reaching the continental slope was found between the high TPF period and the low TPF period. This indicates the persistent rather than episodic influx of sediment resuspension in this area, in accordance with the continuous appearance of benthic and freshwater diatoms and generally high contents of lithogenic matter in the sinking particles during the whole sampling year.

The lateral transport of resuspended sediment in the deep northwestern SCS was also confirmed by another sediment trap observation at the Xisha station (**Figure 8**, 17°24.50′N, 110°55.0′E, two traps mounted at 500 and 1,500 m, with a water depth of 1,690 m), which is ∼27 km to the east of the SCS-NW station. The TPFs at 500 m (**Figure 8**, 128.7 ± 48.8 mg·m^{-2}·d^{-1}) were much lower than those at 1,500 m (322.7 ± 161.6 mg·m^{-2}·d^{-1}) at the Xisha station (Liu et al., 2014; Dong et al., 2016) and lower than those at 1,000 m at the SCS-NW station (531.5 ± 444.5 mg·m^{-2}·d^{-1}), indicating a significant input of laterally transported particles to the deep northwestern SCS subbasin (at least > 500 m). Dong et al. (2016) found that the total particulate phosphorus content in sinking particles at 1,500 m (23.1 ± 11.6 μmol pg^{-1}) was much lower than that at 500 m (47.0 ± 26.3 μmol pg^{-1}) at the Xisha station but very close to that in seafloor sediments (22.73 μmol pg^{-1}, Dang et al., 2013). In addition, in the trap at 1,500 m, they also found a higher percentage of detrital P (46%) and a high percentage (∼58%) of organic P in $CaCO_3$-bound P, which was related to benthic input by carbonate sediments; the percentages of detrital phosphorus and organic phosphorus in $CaCO_3$-bound P are similar to those in the sediment (Dong et al., 2016).

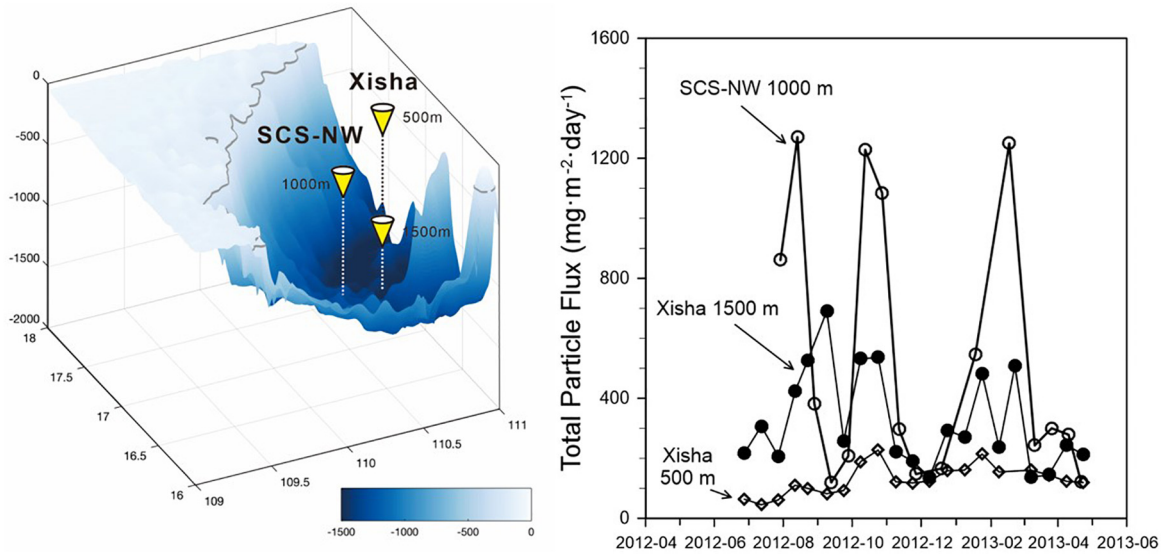

FIGURE 8 | Sketched map of the SCS-NW and Xisha sediment trap moorings and comparison of the total particle fluxes at different depths between the two trap locations.

All the evidence above indicate that large amounts of sediment resuspended from the neighboring continental slope could have been advected into the northwestern SCS subbasin, probably mainly to depths > 500 m. The source region of sinking particles at 500 m at the Xisha station was also analyzed by the LPTM, which showed that none of the particles originated from the seafloor or other submarine obstacles (**Supplementary Dataset 3**), further confirming that the impact of sediment resuspension from the continental slope was mainly in the deep water of the northwestern SCS (>500 m).

Enhanced Input of Resuspended Sediment by Summer Upwelling

The highest probability of particles reaching the continental slope was found in August 2012 (**Figure 7**), when the benthic and freshwater diatom fluxes and abundance were also highest (**Figure 4**), indicating the highest contribution of resuspended sediment to the sinking particles during this period. Assuming that surface productivity in the upper ocean and resuspended sediment from the continental slope were the two sources of the sinking particles collected by the sediment trap at 1,000 m, in which the resuspended sediment with ∼7.8% benthic and freshwater diatoms was the only supplier of benthic and freshwater diatoms, the contribution of diatoms in the resuspended sediment to the diatoms in the sinking particles can be roughly estimated to be ∼18.6 to 88.2%, with the greatest contribution (∼88.2%) during the summer upwelling period.

It is worth noting that the especially large contribution of resuspended sediment also followed the maximum biogenic opal and diatom flux (**Figure 2**) and the maximum flux of coccolithophores (Figure 3 in Ran et al., 2015b), implying significantly enhanced primary productivity in the particle source region in the surface ocean during this period. Zhang et al. (2019) suggested that the enhanced biogenic fluxes were attributed to summer monsoon-induced coastal upwelling off Hainan, which was demonstrated by the low sea surface temperature, high salinity, and high nitrate concentration observed in the coastal area off Hainan (Figure 7 in Zhang et al., 2019). The co-occurrence of enhanced primary productivity and the greatest amount of resuspended sediment during the summer upwelling period further suggest that coastal upwelling induced by the summer monsoon may not only inject nutrients from the subsurface to the surface ocean but also enhance the intrusion of resuspended sediment into the adjacent deep ocean. The capability to erode and transport sediment particles by upwelling was indicated by both observations (Villacieros-Robineau et al., 2013) in the coastal upwelling system of the northwestern Iberian Peninsula and modeling of the upwelling system offshore Walvis Bay, Namibia (Huhn et al., 2007). Our results showed that, being one of the most important hydrodynamic processes at ocean margins, upwelling not only is a key factor controlling the biogeochemical process but also acts as a driving mechanism for sediment transport.

Possible Hydrodynamic Force for Sediment Resuspension

In general, the velocity of the current in the intermediate-deep SCS (<5 cm/s, Shu et al., 2014) was considered too weak to resuspend sediment from the seafloor (Chorley et al., 1984; Chen et al., 2019). However, the persistent input of resuspended sediment into the deep water of the northwestern SCS was indicated by the continuous appearance of benthic and freshwater diatoms, the perpetually high content of lithogenic matter in the sinking particles and the consistent probability of particles originating from the continental slope in the

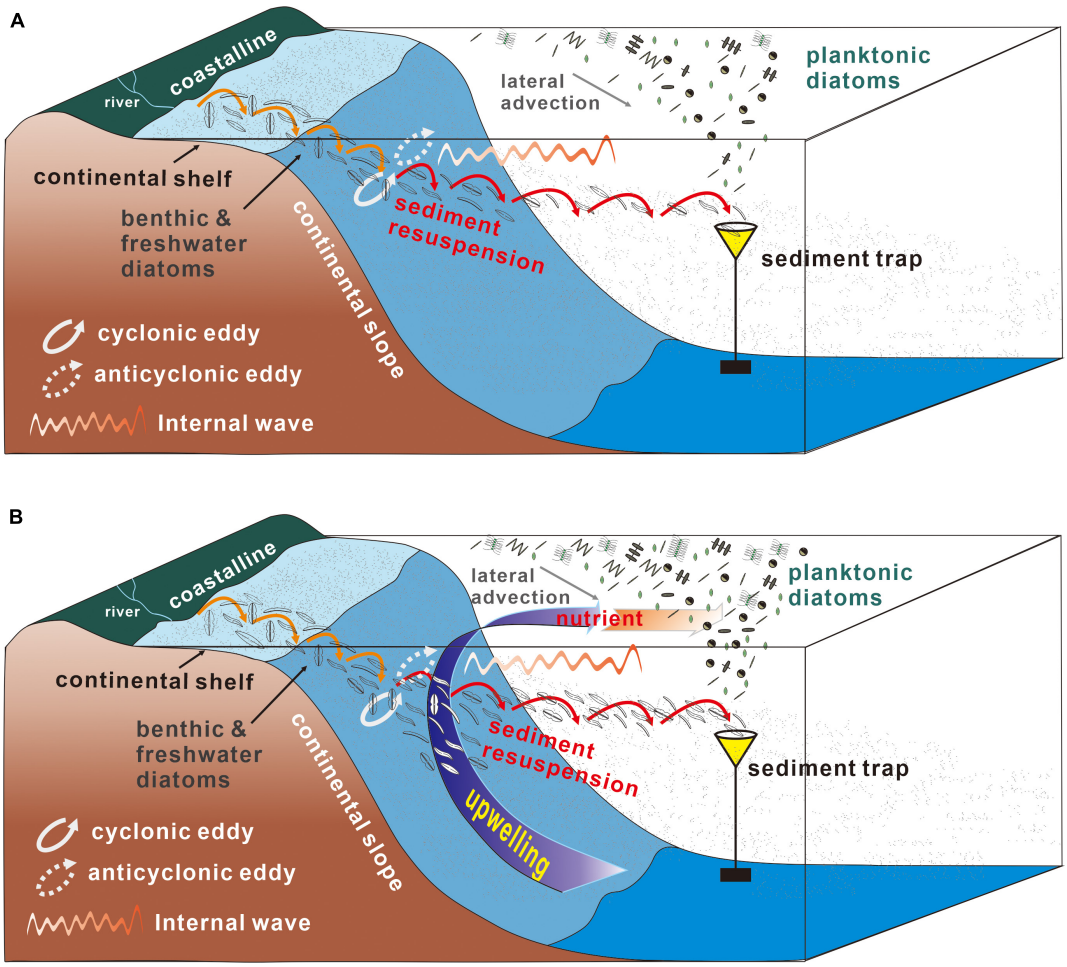

FIGURE 9 | Schematic diagrams of the sources and transport of resuspended sediment from the continental slope to the deep water in the northwestern SCS: **(A)** general case and **(B)** enhanced sediment resuspension by coastal upwelling.

LPTM. This result suggests that persistent sediment resuspension and transportation may be triggered by other hydrodynamic processes in addition to seasonal upwelling.

In addition to the hydrodynamic process of upwelling, it was also suggested that deep-reaching mesoscale eddies and ISWs could dramatically amplify the bottom flow velocity, especially when they pass over rough topography, such as continental breaks, sills or ridges, and erode and resuspend sediments (Bogucki et al., 1997; Zhang et al., 2016; Chen et al., 2019; Jia et al., 2019). Furthermore, sediment resuspension at the seafloor usually results in a bottom nepheloid layer (BNL); subsequently, an intermediate nepheloid layer (INL) could be derived from the BNL after the layers become detached and spread along isopycnal surfaces (Pak et al., 1988). Based on mooring observations in the northern SCS, Jia et al. (2019) observed that both the BNL and the INL are related to ISW-induced sediment resuspension and estimated that ISWs alone could suspend and transport 787 Mt/yr of sediment from the shelf of the northern SCS to the deep sea. Likewise, a deep-reaching mesoscale eddy could also trigger sediment resuspension and, subsequently, a nepheloid layer (Gardner et al., 2017; Chen et al., 2019).

Mesoscale eddies and ISWs have been observed in the northwestern SCS (Wang et al., 2003; Li et al., 2008; Xiu et al., 2010; Chen et al., 2011; Alford et al., 2015; Zhang et al., 2016). Moreover, Xu et al. (2010a,b, 2011, 2013) indicated that ISWs can be generated locally at the continental shelf break in the northwestern SCS as a result of the interaction among internal tides, typhoons, and topography. Although no eddy was found to pass the catchment areas in the upper ocean and the direct impact of eddies may have been minimal during 2012–2013 (not shown), we cannot exclude the possibility of sediment resuspension induced by ISWs or deep eddies that could be generated by seamount wakes (Chen et al., 2015) due to the scarcity of ISW and deep eddy observations in this area. Time-series acoustic Doppler current profiler (ADCP) measurements at the Xisha site (16.85°N, 112.31°E) from May 2009 to September 2010 showed that the current in the subsurface ocean (>300 m) could occasionally reach 0.2–0.3 m/s (20–30 cm/s) (Yang et al., 2015), which is enough to erode and

resuspend the upper slope sediment (Chorley et al., 1984). Recently, an especially high near-bottom current (∼100 m above the seafloor) was also found by ADCP observations in the northern SCS continental slope area, with the highest current speed reaching 80–90 cm/s (yearly average of 50–60 cm/s) as a result of the interaction among internal tides, internal waves, and topography (personal communication in November 2021 with Dr. Chenghao Yang from the Second Institute of Oceanography, MNR). These multiple lines of evidence indicate that high current velocities are possible under the effect of active hydrodynamic processes and complicated topography in the northwestern SCS continental slope. However, more observational data are needed to better understand the hydrodynamic and sedimentary dynamic mechanisms of persistent sediment resuspension in the study area.

CONCLUSION

Diatoms in the sinking particles collected by bottom-tethered time-series sediment traps in the northwestern SCS from July 2012 to May 2013 were analyzed in this work. The frequent appearance of benthic and freshwater diatoms suggest that resuspended sediment was an important contributor to the sinking particles. These diatoms originated from the nearshore area and were repeatedly resuspended and transported long distances to the deep water of the northwestern SCS subbasin. The LPTM using the HYCOM velocity field substantiated the contribution of sediment resuspension and further revealed that the continental slope off Hainan was the nearest source region of the resuspended sediment (**Figure 9**). In particular, the highest contribution of resuspended sediment was found in the summer of 2012. The coincidence between the high input of resuspended sediment and the high primary productivity in the summer monsoon-driven upwelling period indicate that upwelling not only is important in the biogeochemical process but also acts as a driving mechanism for sediment transport in the study area (**Figure 9B**).

This work strongly suggests that resuspended sediment from continental margins should be considered in biological carbon pump observations and estimations. Although resuspended sediment has a relatively low organic carbon content, it could serve as an important input of material to the deep ocean, not only resulting in biased estimates of the biological carbon pump but also causing misunderstandings in palaeoceanographic research in marginal seas, e.g., the SCS. The dynamic mechanism responsible for the generation and lateral transport of and variations in sediment resuspension remains unclear, so continuous and interdisciplinary (hydrological, biogeochemical, sedimentological, etc.) time-series observations in the SCS are necessary in the future.

DATA AVAILABILITY STATEMENT

The original contributions presented in the study are included in the article/**Supplementary Material**, further inquiries can be directed to the corresponding authors.

AUTHOR CONTRIBUTIONS

LR, MW, and JC: conception and design of study. JC: financial support. LR: drafting the manuscript. MW: revising the manuscript. LR, EF, JZ, HL, LZ, and RX: acquisition of data. WM, MW, YW, JC, ZY, and JR: interpretation of data. All authors contributed to the article and approved the submitted version.

FUNDING

This work was funded by the Project of the State Key Laboratory of Satellite Ocean Environment Dynamics, Second Institute of Oceanography, MNR (SOEDZZ2104), the State Key R&D Project of China (2016YFA0601101 and 2016YFC0304105), and the National Natural Science Foundation of China (91128212, 41006034, and 41876123). We acknowledge the support of SML311019006/311020006.

SUPPLEMENTARY MATERIAL

The Supplementary Material for this article can be found online at: https://www.frontiersin.org/articles/10.3389/fmars.2022.819340/full#supplementary-material

Supplementary Dataset 1 | Sampling periods and sinking particle fluxes (total particle fluxes, fluxes of organic matter, $CaCO_3$, biogenic opal and lithogenic matter, and fluxes of diatoms and coccoliths) at the SCS-NW station from July 2012 to April 2013. For the purpose of comparison, the total particle fluxes at 500 and 1,000 m from June 2012 to May 2013 at Xisha station are also included in a separate sheet.

Supplementary Dataset 2 | Diatom assemblages in the sediment trap samples collected at station SCS-NW from July 2012 to April 2013. Information on benthic and freshwater diatoms is shown in a separate sheet.

Supplementary Dataset 3 | LPTM data for particles released with different sinking velocities (sv = m·day^{-1}, 100 m·day^{-1} and 200 m·day^{-1}) at different depths (dp = 500 and 1,000 m) at station SCS-NW.

Supplementary Dataset 4 | Maine chemical components and diatom assemblages in the surface sediments near station SCS-NW.

REFERENCES

Alford, M. H., Peacock, T., MacKinnon, J. A., Nash, J. D., Buijsman, M. C., Centurioni, L. R., et al. (2015). The formation and fate of internal waves in the South China Sea. *Nature* 521, 65–69. doi: 10.1038/nature14399

Bogucki, D., Dickey, T., and Redekopp, L. G. (1997). Sediment resuspension and mixing by resonantly generated internal solitary waves. *J. Phys. Oceanogr.* 27, 1181–1196. doi: 10.1175/1520-0485

Chen, F., Lao, Q., Zhang, S., Bian, P., Jin, G., Zhu, Q., et al. (2020). Nitrate sources and biogeochemical processes identified using nitrogen and oxygen

isotopes on the eastern coast of Hainan Island. *Cont. Shelf Res.* 207:104209. doi: 10.1016/j.csr.2020.104209

Chen, G., Hou, Y., and Chu, X. (2011). Mesoscale eddies in the South China Sea: mean properties, spatiotemporal variability, and impact on thermohaline structure. *J. Geophys. Res.* 116:C06018. doi: 10.1029/2010JC006716

Chen, G., Wang, D., Dong, C., Zu, T., Xue, H., Shu, Y., et al. (2015). Observed deep energetic eddies by seamount wake. *Sci. Rep.* 5:17416. doi: 10.1038/srep17416

Chen, H., Zhang, W., Xie, X., and Ren, J. (2019). Sediment dynamics driven by contour currents and mesoscale eddies along continental slope: a case study of the northern South China Sea. *Mar. Geol.* 409, 48–66. doi: 10.1016/j.margeo.2018.12.012

Chen, J. (2005). *Biogeochemistry of Settling Particles in the South China Sea and Its Significance for Paleo-Environment Studies*. Doctoral dissertation. Shanghai: Tongji University.

Chorley, R. J., Schumm, S. A., and Sugden, D. E. (eds.) (1984). *Geomorphology*. London: Methuen Publishing, 607.

Cummings, J. A., and Smedstad, O. M. (2013). "Variational data assimilation for the global ocean," in *Data Assimilation for Atmospheric, Oceanic and Hydrologic Applications*, Vol. II, eds L. Xu and S. K. Park (Berlin: Springer), 303–343.

Dang, H., Yang, J., Li, J., Luan, X., Zhang, Y., and Gu, G. (2013). Environment-dependent distribution of the sediment nifH-harboring microbiota in the northern South China Sea. *Appl. Environ. Microbiol.* 79, 121–132. doi: 10.1128/AEM.01889-12

Deuser, W. G., Muller-Karger, F. E., Evans, R. H., Brown, O. B., Esaias, W. E., and Feldman, G. C. (1990). Surface-ocean color and deep-ocean carbon flux: how close a connection? *Deep Sea Res. Part A Oceanogr. Res. Pap.* 37, 1331–1343. doi: 10.1016/0198-0149(90)90046-X

Dong, Y., Li, Q. P., Wu, Z., and Zhang, J.-Z. (2016). Variability in sinking fluxes and composition of particle-bound phosphorus in the Xisha area of the northern South China Sea. *Deep Sea Res. Part I* 118, 1–9. doi: 10.1016/j.dsr.2016.10.007

Fredj, E., Carlson, D. F., Amitai, Y., Gozolchiani, A., and Gildor, H. (2016). The particle tracking and analysis toolbox (PaTATO) for Matlab. *Limnol. Oceanogr.* 14, 586–599. doi: 10.1002/lom3.10114

Gardner, W. D., Tucholke, B. E., Richardson, M. J., and Biscaye, P. E. (2017). Benthic storms, nepheloid layers, and linkage with upper ocean dynamics in the western North Atlantic. *Mar. Geol.* 385, 304–327. doi: 10.1016/j.margeo.2016.12.012

Gaye, B., Wiesner, M. G., and Lahajnar, N. (2009). Nitrogen sources in the South China Sea, as discerned from stable nitrogen isotopic ratios in rivers, sinking particles, and sediments. *Mar. Chem.* 114, 72–85. doi: 10.1016/j.marchem.2009.04.003

Herbeck, L. S., Unger, D., Wu, Y., and Jennerjahn, T. C. (2013). Effluent, nutrient and organic matter export from shrimp and fish ponds causing eutrophication in coastal and back-reef waters of NE Hainan, tropical China. *Cont. Shelf Res.* 57, 92–104. doi: 10.1016/j.csr.2012.05.006

Honjo, S., Manganini, S. J., Krishfield, R. A., and Francois, R. (2008). Particulate organic carbon fluxes to the ocean interior and factors controlling the biological pump: a synthesis of global sediment trap programs since 1983. *Prog. Oceanogr.* 76, 217–285. doi: 10.1016/j.pocean.2007.11.003

Hu, J., Kawamura, H., Hong, H., and Qi, Y. (2000). A review on the currents in the South China Sea: seasonal circulation, South China Sea warm current and Kuroshio intrusion. *J. Oceanogr.* 56, 607–624.

Huhn, K., Paul, A., and Seyferth, M. (2007). Modeling sediment transport patterns during an upwelling event. *J. Geophys. Res.* 112:C10003. doi: 10.1029/2005jc003107

Jia, Y., Tian, Z., Shi, X., Liu, J. P., Chen, J., and Liu, X. (2019). Deep-sea sediment resuspension by internal solitary waves in the Northern South China Sea. *Sci. Rep.* 9:12137. doi: 10.1038/s41598-019-47886-y

Lahajnar, N., Wiesner, M. G., and Gaye, B. (2007). Fluxes of amino acids and hexosamines to the deep South China Sea. *Deep Sea Res. Part I* 54, 2120–2144. doi: 10.1016/j.dsr.2007.08.009

Li, H., Wiesner, M. G., Chen, J., Ling, Z., Zhang, J., and Ran, L. (2017). Long-term variation of mesopelagic biogenic flux in the central South China Sea: impact of monsoonal seasonality and mesoscale eddy. *Deep Sea Res. Part I* 126, 62–72. doi: 10.1016/j.dsr.2017.05.012

Li, X., Zhao, Z., and Pichel, W. G. (2008). Internal solitary waves in the northwestern South China Sea inferred from satellite images. *Geophys. Res. Lett.* 35:L13605. doi: 10.1029/2008GL034272

Liu, J., Clift, P. D., Yan, W., Chen, Z., Chen, H., Xiang, R., et al. (2014). Modern transport and deposition of settling particles in the northern South China Sea: sediment trap evidence adjacent to Xisha Trough. *Deep Sea Res. Part I* 93, 145–155. doi: 10.1016/j.dsr.2014.08.005

Liu, K. K., Chao, S. Y., Shaw, P. T., Gong, G. C., Chen, C. C., and Tang, T. Y. (2002). Monsoon-forced chlorophyll distribution and primary production in the South China Sea: observations and a numerical study. *Deep Sea Res. Part I* 49, 1387–1412. doi: 10.1016/S0967-0637(02)00035-3

Liu, K. K., Wang, L. W., Dai, M., Tseng, C. M., Yang, Y., and Sui, C. H. (2013). Inter-annual variation of chlorophyll in the northern South China Sea observed at the SEATS Station and its asymmetric responses to climate oscillation. *Biogeosciences* 10, 7449–7462. doi: 10.5194/bg-10-7449-2013

Ma, W., Xiu, P., Chai, F., Ran, L., Wiesner, M. G., and Xi, J. (2021). Impact of mesoscale eddies on the source funnel of sediment trap measurements in the South China Sea. *Prog. Oceanogr.* 194:102566. doi: 10.1016/j.pocean.2021.102566

Pak, H., Ronald, J., Zaneveld, V., and Kitchen, J. (1988). Intermediate nepheloid layers observed off Oregon and Washington. *J. Geophys. Res.* 85:12. doi: 10.1029/JC085iC11p06697

Priyadarshani, W. N. C., Ran, L., Wiesner, M. G., Chen, J., Ling, Z., Yu, S., et al. (2019). Seasonal and interannual variability of coccolithophore flux in the northern South China Sea. *Deep Sea Res. Part I* 145, 13–30. doi: 10.1016/j.dsr.2019.01.004

Ran, L., Chen, J., Wiesner, M. G., Ling, Z., Lahajnar, N., and Yang, Z. (2015a). Variability in the abundance and species composition of diatoms in sinking particles in the northern South China Sea: results from time-series moored sediment traps. *Deep Sea Res. Part II* 122, 15–24. doi: 10.1016/j.dsr2.2015.07.004

Ran, L., Beaufort, L., Li, H., Chen, J., Wiesner, M., Yang, Z., et al. (2015b). Coccolith downward fluxes and species compositions recorded in the sediment trap in the northwest South China Sea. *Haiyang Xuebao* 37, 11–18.

Shen, J., Jiao, N., Dai, M., Wang, H., Qiu, G., and Chen, J. (2020). Laterally transported particles from margins serve as a major carbon and energy source for dark ocean ecosystems. *Geophys. Res. Lett.* 47:e2020GL088971. doi: 10.1029/2020GL088971

Shu, Y., Xue, H., Wang, D., Chai, F., Xie, Q., Yao, J., et al. (2014). Meridional overturning circulation in the South China Sea envisioned from the high-resolution global reanalysis data GLBa0. 08. *J. Geophys. Res.* 119, 3012–3028. doi: 10.1002/2013JC009583

Siegel, D. A., and Deuser, W. G. (1997). Trajectories of sinking particles in the Sargasso Sea: modeling of statistical funnels above deep-ocean sediment traps. *Deep Sea Res. Part I* 44, 1519–1541. doi: 10.1016/S0967-0637(97)00028-9

Siegel, D. A., Fields, E., and Buesseler, K. O. (2008). A bottom-up view of the biological pump: modeling source funnels above ocean sediment traps. *Deep Sea Res. Part I* 55, 108–127. doi: 10.1016/j.dsr.2007.10.006

Tan, S., Zhang, J., Li, H., Sun, L., Wu, Z., and Wiesner, M. G. (2020). Deep ocean particle flux in the northern South China Sea: variability on intra-seasonal to seasonal timescales. *Front. Earth Sci.* 8:74. doi: 10.3389/feart.2020.00074

Villacieros-Robineau, N., Herrera, J. L., Castro, C. G., Piedracoba, S., and Roson, G. (2013). Hydrodynamic characterization of the bottom boundary layer in a coastal upwelling system (Ría de Vigo, NW Spain). *Cont. Shelf Res.* 68, 67–79. doi: 10.1016/j.csr.2013.08.017

Wang, A., Du, Y., and Qi, Y. (2015). Correlation between subsurface high-salinity water in the northern South China Sea and the North Equatorial Current–Kuroshio circulation system from HYCOM simulations. *Ocean Sci.* 11, 305–312. doi: 10.5194/os-11-305-2015

Wang, G., Su, J., and Chu, P. C. (2003). Mesoscale eddies in the South China Sea observed with altimeter data. *Geophys. Res. Lett.* 30:2121. doi: 10.1029/2003GL018532

Wang, L., Huang, B., Chiang, K. P., Liu, X., Chen, B., and Xie, Y. (2016). Physical-biological coupling in the western South China Sea: the response of phytoplankton community to a mesoscale cyclonic eddy. *PLoS One* 11:e0153735. doi: 10.1371/journal.pone.0153735

Wang, L., Huang, B., Laws, E. A., Zhou, K., Liu, X., Xie, Y., et al. (2018). Anticyclonic eddy edge effects on phytoplankton communities and particle export in the northern South China Sea. *J. Geophys. Res.* 123, 7632–7650. doi: 10.1029/2017JC013623

Wang, P., Li, Q., and Dai, M. (2015). The south china sea deep: introduction. *Deep Sea Res. Part II* 122, 1–5. doi: 10.1016/j.dsr2.2015.11.004

Wang, S. H., Hsu, N. C., Tsay, S. C., Lin, N. H., Sayer, A. M., Huang, S. J., et al. (2012). Can Asian dust trigger phytoplankton blooms in the oligotrophic northern South China Sea? *Geophys. Res. Lett.* 39:L05811. doi: 10.1029/2011GL050415

Waniek, J. J., Koeve, W., and Prien, R. D. (2000). Trajectories of sinking particles and the catchment areas above sediment traps in the northeast Atlantic. *J. Mar. Res.* 58, 983–1006. doi: 10.1357/002224000763485773

Waniek, J. J., Schulz-Bull, D. E., Blanz, T., Prien, R. D., Oschlies, A., and Müller, T. J. (2005). Interannual variability of deep water particle flux in relation to production and lateral sources in the northeast Atlantic. *Deep Sea Res. Part I* 52, 33–50. doi: 10.1016/j.dsr.2004.08.008

Wekerle, C., Krumpen, T., Dinter, T., Von Appen, W., Iversen, M. H., and Salter, I. (2018). Properties of sediment trap catchment areas in fram strait: results from lagrangian modeling and remote sensing. *Front. Mar. Sci.* 5:407. doi: 10.3389/fmars.2018.00407

Wiesner, M. G., Zheng, L., Wong, H. K., Wang, Y., and Chen, W. (1996). "Fluxes of particulate matter in the South China Sea," in *Particle Flux in the Ocean*, eds V. Ittekkot, P. Schäfer, P. Depetris, and S. Honjo (Chichester: John Wiley & Sons Ltd), 293–299.

Wu, Y., Bao, H. Y., Unger, D., Herbeck, L. S., Zhu, Z. Y., Zhang, J., et al. (2013). Biogeochemical behavior of organic carbon in a small tropical river and estuary, Hainan, China. *Cont. Shelf Res.* 57, 32–43. doi: 10.1016/j.csr.2012.07.017

Wyrtiki, K. (1961). Physical oceanography of the Southeast Asian waters. *Naga Rep.* 2:195.

Xiu, P., Chai, F., Shi, L., Xue, H., and Chao, Y. (2010). A census of eddy activities in the South China Sea during 1993–2007. *J. Geophys. Res.* 115:C03012. doi: 10.1029/2009JC005657

Xu, Z. H., Yin, B. S., and Hou, Y. J. (2011). Response of internal solitary waves to tropical storm Washi in the northwestern South China Sea. *Ann. Geophys.* 29, 2181–2187.

Xu, Z., Yin, B., and Hou, Y. (2010a). Highly nonlinear internal solitary waves over the continental shelf of the northwestern South China Sea. *Chinese J. Oceanol. Limnol.* 28, 1049–1054. doi: 10.1007/s00343-010-9018-1

Xu, Z., Yin, B., Hou, Y., and Xu, Y. (2013). Variability of internal tides and near-inertial waves on the continental slope of the northwestern South China Sea. *J. Geophys. Res.* 118, 197–211. doi: 10.1029/2012JC008212

Xu, Z., Yin, B., Hou, Y., Fan, Z., and Liu, A. K. (2010b). A study of internal solitary waves observed on the continental shelf in the northwestern South China Sea. *Acta Oceanol. Sin.* 29, 18–25. doi: 10.1007/s13131-010-0033-z

Yan, Y., Wang, G., Xue, H., and Chai, F. (2019). Buoyancy effect on the winter South China Sea western boundary current. *J. Geophys. Res.* 124, 6871–6885. doi: 10.1029/2019JC015079

Yang, L., Wang, D., Huang, J., Wang, X., Zeng, L., and Shi, R. (2015). Toward a mesoscale hydrological and marine meteorological observation network in the South China Sea. *Bull. Am. Meteorol. Soc.* 96, 1117–1135. doi: 10.1175/BAMS-D-14-00159.1

Yu, Y., Wang, Y., Cao, L., Tang, R., and Chai, F. (2020). The ocean-atmosphere interaction over a summer upwelling system in the South China Sea. *J. Mar. Syst.* 208:103360. doi: 10.1016/j.jmarsys.2020.103360

Yu, Y., Xing, X., Liu, H., Yuan, Y., Wang, Y., and Chai, F. (2019). The variability of chlorophyll-a and its relationship with dynamic factors in the basin of the South China Sea. *J. Mar. Syst.* 200:103230. doi: 10.1016/j.jmarsys.2019.103230

Zhang, J., Li, H., Xuan, J., Wu, Z., Yang, Z., Wiesner, M. G., et al. (2019). Enhancement of mesopelagic sinking particle fluxes due to upwelling, aerosol deposition, and monsoonal influences in the Northwestern South China Sea. *J. Geophys. Res.* 124, 99–112. doi: 10.1029/2018JC014704

Zhang, Z., Tian, J., Qiu, B., Zhao, W., Chang, P., Wu, D., et al. (2016). Observed 3D structure, generation, and dissipation of oceanic mesoscale eddies in the South China Sea. *Sci. Rep.* 6, 1–11. doi: 10.1038/srep24349

Zhang, Z., Zhao, W., and Liu, Q. (2010). Sub-seasonal variability of Luzon strait transport in a high resolution global model. *Acta Oceanol. Sin.* 29, 9–17. doi: 10.1007/s13131-010-0032-0

Zhou, K., Dai, M., Kao, S. J., Wang, L., Xiu, P., and Chai, F. (2013). Apparent enhancement of 234Th-based particle export associated with anticyclonic eddies. *Earth Planet. Sci. Lett.* 381, 198–209. doi: 10.1016/j.epsl.2013.07.039

Conflict of Interest: The authors declare that the research was conducted in the absence of any commercial or financial relationships that could be construed as a potential conflict of interest.

Publisher's Note: All claims expressed in this article are solely those of the authors and do not necessarily represent those of their affiliated organizations, or those of the publisher, the editors and the reviewers. Any product that may be evaluated in this article, or claim that may be made by its manufacturer, is not guaranteed or endorsed by the publisher.